

# Improving Seismometer Performance at Low Frequencies using newly discovered physics

Randall D. Peters  
Mercer University

June 2005

## Abstract

Modern commercial seismometers are without equal in their ability to study earth motions in the frequency range from 30 mHz to 10 Hz. In the increasingly important lower range from 1 mHz to 30 mHz, their sensitivity is severely limited. These limitations are discussed in terms of recent physics discoveries concerned with internal friction. It is shown that the low-frequency performance can be significantly improved by using a different (i) style of capacitive sensor, and (ii) method of force-feedback. Advantages of these novel changes are illustrated with a modified long-period Sprengnether vertical seismometer that was previously part of the WWSSN.

## 1 Background

Modern seismometers have evolved along a path whose direction was significantly influenced by the work of Michael Faraday. A variety of detectors have been employed to sense movement of the inertial mass of the instrument relative to the frame. These involve diverse types of sensors, whose characteristics are classified mainly as either mechanical, electromagnetic, or optical. The mechanical types are inferior for reason of friction at contact points, such as a stylus that writes on a blackened drum.

The most successful early form of electromagnetic detector was one that employs a coil of wire and a magnet. The magnet is fixed to the frame of the instrument, and the coil moves with the mass. (The mass cannot be allowed to move because of adverse interaction with the earth's field.) Their relative motion causes the magnetic flux through the coil to change in time, and its rate of change determines the voltage appearing across the ends of the wire used to wind the multi-turn coil. The very nature of this Faraday's law detector is such that the voltage generated is proportional to the velocity of the mass. As compared to a measurement of mass position, velocity measurement is a poor choice for those concerned with improving low-frequency performance. This point is discussed in detail later.

Most modern seismometers of the type employed in the Global Seismographic Network have used a capacitive sensor to measure mass position. Commonly of the type that is referred to as differential, it comprises two capacitors that change in opposite manner in response to mass motion. Built with three closely spaced, parallel plate electrodes; the two outer plates are fixed, and the inner plate moves so that if one of the capacitors increases by a small amount, then the other capacitor decreases (ideally) by the same amount. Use of this differential arrangement improves overall sensitivity, in part by providing a better common mode rejection for the electronics connected to the sensor. Certainly the choice, in general, of a capacitance sensor has been a proper one, because among readily available non-invasive sensor types, none is better presently qualified for seismic studies.

A better choice than the (half) differential capacitive sensor described above, and which is universally used in commercial seismometers, would be one of the 'fully differential' capacitive sensors developed in recent years. The increased symmetry of the fully differential detector yields twice the sensitivity for the same electrode area and a better common mode rejection ratio. Thus the performance of seismometers could readily be improved by more than a factor of two, based on just this change alone. We will see that there are other improvements allowed by changing to a different architecture for the sensor;

it allows a ‘soft’ force-feedback which is better suited to monitoring low-frequency signals than is the ‘force-balance’ methods commonly used.

One might argue that a magnetic detector would be equally viable; for example, in the form of a linear variable differential transformer (LVDT). As Erhard Wielandt has pointed out [1], the signal to noise ratio of an LVDT is inferior (by as much as two orders of magnitude) to that of a capacitive detector. This inferiority derives from magnetic domain noise related to the Barkhausen effect, involving the granular nature of ferromagnetism.

## 1.1 Types of capacitive sensor

The capacitance of a two terminal device (lumped circuit element) is of the form

$$C = \epsilon_0 A/d \tag{1}$$

where  $\epsilon$  is the permittivity of the material between parallel electrode plates, which for air of the usual instrument is close enough to the free space value that the subscript zero has been indicated; i.e.,  $\epsilon_0 = 8.85 \times 10^{-12} Nm^2/C^2$ . The area of each of the two plates is  $A$  and the spacing between them is  $d$ . This equation is an excellent approximation for the capacitance when the gap spacing  $d$  is small, so that fringe electric fields may be ignored.

It is generally desirable to operate with as conveniently small a value of  $d$  as possible, because the sensitivity of the unit as a detector is inversely proportional to  $d$ . To state the matter more precisely, the sensitivity is determined by the size of the electric field between the plates, which increases as  $d$  decreases, for a given drive voltage across the plates.

### 1.1.1 Variable-gap detector

Differential capacitive detectors of modern commercial (research-grade) seismometers operate on the basis of gap-spacing variation; i.e.,

$$C(t) = \epsilon_0 A/d(t) \tag{2}$$

For adequate sensitivity, the nominal average spacing must be small,  $d_0 < 1.0 \text{ mm}$ . This stringent requirement on spacing between electrodes having an area  $> 10 \text{ cm}^2$ , has influenced the modus operandus of these instruments. It is a style of force-feedback referred to as ‘force-balance’, in which ‘hard’ coupling is used to keep the inertial mass virtually fixed in position. Instead of monitoring the position or velocity of the inertial mass as in the early days of seismometry, they now monitor the ‘error’ signal generated by the feedback-balance network, i.e., the current supplied to a transducer used to keep the mass virtually stationary.

### 1.1.2 Variable-area detector

An alternative to gap-variation is a capacitive sensor that employs area-variation; i.e.,

$$C(t) = \epsilon_0 A(t)/d \tag{3}$$

We will see that the (ideally fixed) spacing  $d$  between electrodes for this case can be conveniently increased by using an array-form of sensor, and constraints to mass movement can be relaxed greatly as compared to an instrument which operates according to eq(2).

## 2 Friction in general

Ubiquitous friction, which exists in a variety of forms, places a limit on the sensitivity of a seismometer. Although physicists impress the world with their knowledge of certain esoterica, we know almost nothing from first principles about friction [2].

## 2.1 Coulomb friction

The form of friction most commonly recognized is the one involving solid surfaces that slide against each other. Known as Coulomb friction, it was first studied by Leonardo DaVinci and later by Charles Augustin Coulomb, who is best known for his law of electrostatic forces. As the primary cause for limited performance of early detectors using mechanical linkages, the magnitude of the kinetic friction force is (approximately) proportional to the normal contact force between the surfaces, and it is independent of the surface area of contact and the speed of relative motion between the surfaces. When present as the primary loss of energy in a mechanical oscillator, it causes the turning points of the motion to decline along a straight line, as opposed to the exponential decline of other common types. Unlike viscous friction, Coulomb friction is nonlinear, by virtue of the ‘signum’ function needed to mathematically describe its damping influence on an oscillator. The direction of this friction force is opposite the direction of the velocity, but the magnitude of the force is independent of the velocity magnitude. As a damping force, it is thus described by  $\vec{f} = -|\text{constant}| \times \text{sgn}(\vec{v})$

## 2.2 Viscous friction

Viscous friction is present as an external-to-the-object retarding force for an object moving relative to a fluid, whether gas or liquid. It is the only common friction type that can be described by linear mathematics when it comes to damping of the ‘simple’ harmonic oscillator [3].

Although it frequently yields to a linear description, fluid friction is generally far more complex than the overly-idealized, common assumption of a drag force proportional to velocity and involving only the viscosity [4]. In reality, the force of viscous friction generally depends on density of the fluid as well as its viscosity. The damping coefficient  $\beta$  used in the classical equation  $\ddot{x} + 2\beta\dot{x} + \omega_0^2x = 0$  should never be referred to as a ‘constant’. It should also be noted that the subscript zero to distinguish between the undamped and damped eigenfrequencies is practically unnecessary, since the damping redshift is generally (perhaps always) too small to actually be measured in the midst of noise. This is an example of the uncertainty principle (of Heisenberg fame in the analogous quantum mechanical case). It should also be noted, that in the case of hysteretic damping, there is no theory-predicted damping redshift.

The Reynolds number [5] is rarely small enough for purely laminar flow, free from vortices. Thus there are ‘history’ features to the drag that imply ‘friction at the mesoscale’ [2], as the mass passes back and forth through vortices that it generated at earlier times.

Fluid friction at higher speeds is nonlinear in the velocity; the drag force on vehicles at nominal speeds of travel, for example, is quadratic and not linear in the velocity. A swinging pendulum, such as a grandfather clock, experiences both linear and nonlinear fluid damping from the air. For seismometers with a gap-varying capacitive detector, the damping at large amplitudes is mainly linear (viscous) and derives from air flowing through the plates of the closely spaced capacitive sensor. To reduce this viscous damping, holes are oftentimes drilled through the electrode plates of the gap-varying type of detector.

At low amplitudes hysteretic damping becomes increasingly important and is now discussed.

## 2.3 Hysteretic friction

The most important form of friction for seismometers operating at low frequency and low amplitude is internal (hysteretic) friction. It derives from periodic flexure occurring in solid, load-bearing members, and is especially important as an anelastic presence in the spring of a vertical instrument.

Hysteretic damping is inherently nonlinear, even though it masquerades as viscous friction. It causes an exponential free-decay, yet the frequency dependence of the quality factor  $Q$  of an oscillator is distinctly different when regulated by hysteretic as opposed to viscous damping.  $Q$  is defined by

$$Q = 2\pi \frac{E}{|\Delta E|} \quad (4)$$

where  $E$  is the mechanical energy of the oscillator at a specified time and  $\Delta E$  is the energy lost per cycle to friction at that time.

For viscous damping  $Q \propto \omega$ , with  $\omega = 2\pi/T$  where  $T$  is the period of oscillation. On the other hand, for hysteretic damping,  $Q \propto \omega^2$ . A perfect example of simple harmonic oscillation with ‘viscous’

damping is that of an RLC electrical circuit. Its equation of motion in terms of the charge  $q$  on the capacitor is given by

$$\ddot{q} + \frac{R}{L}\dot{q} + \frac{q}{LC} = 0 \quad (5)$$

and it can be shown that  $Q = \omega L/R$ . Thus the equation of motion can be rewritten in the canonical linear form

$$\ddot{q} + \frac{\omega}{Q}\dot{q} + \omega_0^2 q = 0 \quad (6)$$

where  $\omega_0^2 = \frac{1}{LC}$  and  $Q = \frac{L}{R}\omega$ . As noted earlier  $\omega = \sqrt{\omega_0^2 - (\frac{R}{2L})^2}$  differs by a very small amount from  $\omega_0$ . For  $Q > 5$ ,  $\frac{\omega}{\omega_0} \approx 1 - \frac{1}{8Q^2}$  to an excellent approximation. At  $Q = 5$  the ‘damping redshift’ is only 0.5%, and the frequency for this case is so ill-defined, for the rapidly declining sinusoid, that the shift is not measurable by spectral means. As noted earlier, to measure the shift by means of a theoretical fit to the data, the bandpass of the electronics must be opened significantly, to avoid distortion of the signal. This introduces Johnson noise that causes the residuals between theory and experiment to be large. Again we find that the theoretical expression for the shift can not be validated. Consequently, we deduce that the damping redshift is not practically meaningful.

We see from eq(6) that  $Q \propto \omega$ , the hallmark of viscous damping. The form of the equation is clearly appropriate to the description of the RLC circuit, and also of some mechanical oscillators; where the damping is dominated by viscous friction. On the basis of units alone, however, a problem is observed with the use of eq(6) to model an oscillator dominated by hysteretic damping in which  $Q \propto \omega^2$ .

### 3 Recent Internal Friction Discoveries

It is known from a variety of experiments, beginning with those of Kimball and Lovell [6], that with hysteretic damping  $Q \propto \omega^2$ . Even the studies of Gunar Streckeisen as a student, with a LaCoste spring vertical seismometer, demonstrated hysteretic damping. Free-decay data that he collected (including periods in excess of 100 s) show clearly that the damping of his instrument at lower frequencies was of the form  $Q \propto \omega^2$  [7].

A number of recent experiments by Peters have demonstrated that hysteretic friction is fundamentally nonlinear. Use of the modified Coulomb damping model [4] for this universal form of solid attenuation, yields the following damped harmonic oscillator equation

$$\ddot{x} + \frac{\pi \omega_d}{4} \frac{\omega_d}{Q} \sqrt{\omega_d^2 x^2 + \dot{x}^2} \operatorname{sgn}(\dot{x}) + \omega^2 x = 0 \quad (7)$$

where the subscript  $d$  on  $\omega$  identifies the drive frequency. For free-decay, the drive frequency is the natural frequency  $\omega$  of the oscillator; i.e.,  $\omega_d \rightarrow \omega$ .

It can be shown for this equation of motion that  $Q \propto \omega^2$ [8]. Using the orthogonality properties of the harmonic functions, sine and cosine, it can also be shown that only the fundamental of the fourier series describing the friction force is important in determining the log-decrement (and thus the  $Q$ ) of an exponential free-decay.

The friction waveform predicted by eq(7) is approximately a square wave, similar to Coulomb friction; except that the amplitude of the friction force is proportional to the amplitude of the motion. The reason for the  $\frac{\pi}{4}$  term is that the fundamental of a square wave is the reciprocal of this quantity times the amplitude of the wave.

A conceptual appreciation for the internal friction is realized by recognizing that it derives from rearrangement of polycrystalline grains in the metal of a spring as it changes its strain state. In other words, the anelasticity responsible for energy conversion to heat is the result of atomic rearrangements. The amount of the inter-grain ‘sliding friction’ goes as the square root of the energy

$E = \frac{1}{2}m \dot{x}^2 + \frac{1}{2}m\omega^2 x^2$ . It is seen from eq(7) that the effective friction force is proportional to  $\sqrt{\frac{2E}{m}}$

## 4 Importance of Hysteretic damping to a Seismometer

Strain of the spring in a vertical seismometer is inherent to the instrument's function. If the spring were of Hooke's law (ideal) type, it would be frictionless. Real materials never obey Hooke's law, except perhaps for displacements measured in a few angstroms, as noted by studies using scanning tunneling microscopes [9]. As the mass moves in (nearly) harmonic motion (assuming an 'underdamped' instrument) in response to an earth impulsive excitation, the spring of the seismometer cycles around a hysteresis loop of stress versus strain. It should also be noted that the load bearing members of a horizontal seismometer (whether of the 'garden-gate' (Lehman) variety or a folded pendulum, as examples) also experience energy loss that is part of such hysteresis.

Although it is tempting to believe that friction effects have been virtually eliminated with the advent of new sensor technologies, this is far from true. The enormous complexity that is observed, when one looks carefully at the properties of a modern seismometer—results largely from the defect properties of the spring that is the quintessential component of a vertical seismometer. We will see that stress-strain hysteresis in this spring plays a critical role in determining the sensitivity of seismometers operating at mHz frequencies.

A type of universal friction in which the effective force of resistance to the motion is independent of frequency, hysteretic internal friction is responsible for an exponential free-decay. Its influence is so similar to that of viscous damping, that it often is incorrectly labeled as linear in the velocity.

The zero-length LaCoste spring of earlier WWSSN instruments, has been mainly replaced by the astatic spring of the modern seismometer (patented by Wielandt and used by Streckeisen) . A significant mechanical amplification is realized by the use of these springs, allowing the instrument to become highly sensitive to earth motions at frequencies in the range from 30 mHz to 10 Hz. They are sometimes described as having sensitivity equal to a very long pendulum, assuming that adverse consequences of the increased length are not an issue. The increased performance (when not limited by friction) is a consequence of the fact that the sensitivity of an accelerometer to acceleration  $a$  is proportional to the square of its natural period. This is easily demonstrated for the perfect (Hooke's law) spring as follows:

$$F = -k x \quad \rightarrow \quad Sens. = \frac{\Delta x}{\Delta a} = -\frac{T^2}{4\pi^2} = -\frac{1}{\omega^2} \quad (8)$$

where the connection between spring constant  $k$  and period  $T = 2\pi/\omega$  has been used (from the solution to the equation of motion for the mass-spring simple harmonic oscillator without damping; i.e.,  $m\ddot{x} + kx = 0$ ).

As the period of oscillation lengthens, and the amplitude of motion decreases; a point is eventually reached where the mesoanelastic complexity of materials common to seismic instruments becomes undeniably visible [10]. With softer (malleable) materials that are not suitable for the construction of a seismometer, it is much easier to demonstrate the complexities, while operating at much larger amplitudes[11].

This place of incipient complexity is the very place of increasing importance to geoscience—the place where low-frequency earth dynamics involving 'noise' driven eigenmodes can be studied. Unfortunately, it is also the very place where the mesodynamic properties of a seismometer make for complexity of instrument dynamics. The response of the instrument to a stimulus is no longer the classical harmonic oscillator with viscous (linear) damping. The system is more than simply nonlinear, such as to disallow the use of convolution and thus transform techniques in the mathematical treatment (superposition no longer possible). Its behavior can be cause for much confusion, assuming that the earth motions we wish to study are even detectable to begin with.

### 4.1 1/f Noise

Real systems can demonstrate 'white' noise, in which there is no frequency dependence. Examples include (i) bit-resolution limitations of an analog to digital converter, and (ii) the bandpass noise of thermal type in resistors of electronics; where it is referred to as Johnson noise.

Solid state electronic amplifiers show noise increase with decreasing frequency, in which a plot of dB versus log frequency typically has a slope -1/f. It is thus referred to as 1/f noise. Of all noise types, this is the one most universal.

Other than very high-Q systems of non-metallic type, mechanical oscillators always demonstrate 1/f noise. Peters has postulated that this noise originates at the mesoscale [2]. It is a consequence of mesoanelastic complexity having similarities to the Barkhausen effect (discrete; i.e., ‘jerky’ behavior because of defects). The 1/f noise is generated as a consequence of the natural organizational characteristics of these defects. To better appreciate the measurement conundrum resulting from the physics of these processes, we now discuss self organized criticality.

## 5 Self-Organized Criticality

It is quite possible that seismologists were the first to seriously encounter self organized criticality (SOC), because of the log-log graphics common to the representation of data influenced by SOC. A log-log plot of earthquake frequency of occurrence versus earthquake magnitude (Gutenberg-Richter relationship) is a classic example of the phenomenon that has become well known to the physics world through the work of Bak, Tang, and Wiesenfeld[12].

Not only does the earth exhibit features of SOC at the megameter scale, but a seismometer exhibits similar things at the centimeter scale. (This should not be a startling revelation to the reader, since one of the hallmarks of SOC is its invariance to scale.) It is well known, for example, that transient consequences of a major disturbance to an instrument must be allowed to ‘settle out’. The settling process is one that involves creep, in which defects of the metal organize themselves in the direction of a type of ‘stable’ point resisting further creep. Actually the acquired state is better described as metastable, since a change in temperature or stress will, if sufficiently large, disrupt the ‘equilibrium’. It is interesting that the SOC processes that are part of metastable attainment can be accelerated by impulsive blows to the instrument. For example, Wielandt has mentioned how a seismometer may be brought to operational status more quickly by hammering on the pier, “a procedure that is recommended in each new installation” [1] (section “Transient disturbances” in “Instrumental self-noise”).

## 6 Force-balance versus ‘soft’ force-feedback

It is the opinion of this author that force-balance, of the type used in commercial seismometers, is detrimental to the instrument’s performance at low frequencies. Reasoning for this conclusion is related to the matter of SOC. The granular properties of SOC are not readily observed at higher frequencies where the energies of oscillation are large enough to average over many discrete events. At low frequencies, internal friction, and especially its discrete character, becomes more important. It is believed that to seriously constrain the mass from motion is to detrimentally hamper the mechanisms of SOC to which the material tries to respond. Allowed to move, it naturally evolves toward regions of greater stability that provide improved performance.

Although some feedback is necessary to keep an instrument from ‘going to the rails’ electronically when operating at high sensitivity, it is hypothesized that the influence of mesoanelastic complexity can be reduced by working with much smaller forces than those required for force-balance. To test this hypothesis, an unconventional form of feedback was employed for use on a modified Sprengnether instrument. The modified instrument is pictured in Fig. 1, and the capacitive sensor used in place of the original (Faraday law) detector is pictured in Fig. 2. The damping subsystem used during operation would normally also be visible in this picture. The forces employed in a force-balance instrument are so large that no external source of damping is necessary. Placement in the complex-plane, of the pole and zeroes of the network, is such that the feedback circuit itself causes the instrument to behave like a classical instrument whose damping is close to the desired critical value. With the small feedback forces of the modified Sprengnether it is necessary to supply a damper, in the form of an eddy-current subsystem. It is a damper whose magnets were taken from a computer hard-drive, and they are held together with a structure built of soft iron rectangular pieces of 1/4 in. thickness. Between the open pole faces is a gap of about 2 mm, inside which a small copper sheet moves. This copper sheet was glued on one end to the inside vertical face of the left lead-mass shown in Fig. 2. The sheet is thin enough, and the width small enough, that it never mechanically contacts anything. With a length sufficient to extend all the way through the pole face region, damping close to critical is realized.

Although the Faraday law unit is still used, it is for an entirely different purpose than the original design. It is now employed to function as an actuator. Its magnet housing (outer heavy ferrous cylinder used for flux closure) is visible in the Fig. 1 photograph as the dark cylinder. Its companion coil (not visible, surrounded by the ferrous housing), is wound on a plastic spool attached to the frame piece with the big holes, that moves in concert with the two lead cylinders that constitute the inertial mass of the instrument. The feedback provided by the capacitive sensor and the magnet/coil actuator is unconventional, in that it does not use a derivative function. Unlike commercial instruments, which use both differentiation and integration; the present feedback system uses only a long-time-constant integration, as illustrated in Fig. 3.

Shown in Fig. 4 is a graph that compares instrument response below resonance, for sensors of either (i) displacement type, or (ii) velocity type. The greater fall-off rate of the velocity sensor (additional 20 dB/decade) makes velocity sensing a poor choice for low-frequency purposes.

## 7 Capacitive Sensor

The sensor of this modified instrument is fully differential and patented in the U.S. with the name “symmetric differential” [13]. As noted earlier, it functions on the basis of area variation, as illustrated in Fig. 3. The grounded electrode that moves with the seismic mass, is situated between parallel static electrodes. Charge cannot be induced through this grounded plate, so the four capacitors of the bridge circuit change in symmetric manner, according to the position of the moving electrode. It is a ‘fully active’ capacitive bridge that has been described by some as a form of ‘shadow’ sensor.

It can be shown that the sensitivity of an idealized symmetric differential capacitive (SDC) sensor is inversely proportional to the width of the moving electrode (analysis that ignores the influence of output reactance in the Thevenin equivalent circuit). By shrinking this dimension toward zero, one could in principle attain very high sensitivity. In reality, there is an opposing loss of sensitivity of capacitive type. Because of the output capacitance of the sensor, and the input capacitance of the amplifier to which it is connected; the sensitivity actually decreases as the indicated electrode dimension is decreased. This results because the open-circuit voltage of the sensor is ‘divided’ between the sensor’s output capacitance and the amplifier’s input capacitance.

The way to overcome the voltage-divider limitation is to work with an array and maintain the output capacitance nearly fixed as the dimension is reduced. By placing several individual SDC detectors in electrical-parallel, a large increase in sensitivity can be effected, as compared to a single capacitive unit.

The number of elements in the array is determined by the mechanical dynamic range of the instrument (and one’s fabrication abilities). Since the amount of seismic mass movement is typically quite small, the number could be made considerably larger than the six elements shown in Fig. 2. The small number presently employed is a consequence primarily of the method of manufacture. The electrodes were formed from printed circuit board; with various insulator strips generated by hand, using a file and a straightedge to remove copper from the fiberglass backing. It is a testament to the versatility of this sensor that it is able to perform remarkably well, in spite of the crudeness of its construction. The truth of this statement will be demonstrated in example data records that follow.

To those with training in optics, the capacitive array may bring to mind various components that work on the basis of interference. As the resolution of a multi-slit grating is greater than that of a pair of slits (Young’s experiment); in somewhat similar manner, an array form of the SDC sensor has a greater sensitivity than is possible with a single-element SDC sensor. Of course, the mechanical dynamic range decreases proportionately, as the number of elements in the array increases. In the case of a seismometer, the tradeoff between sensitivity and displacement range will be governed by the maximum displacement of the seismic mass. If force balance were employed the range would be very small. As implied by the premise of this article, larger range (in excess of 1 mm) will be allowed to improve low frequency performance.

## 8 Examples of Instrument Capabilities

All data were collected with the instrument resting on a pier that is unconventional. It comprises a (i) fairly massive ‘composite table top’, sitting at its center on the flat-bottom (approx. 8-in dia.) of a (ii) steel high-pressure bottled gas cylinder buried 4-ft vertically in the ground (inverted orientation).

The instrument has not been yet carefully calibrated, using an optical lever with the front-surface mirror visible in Fig. 2. In previous studies, where the electronics was slightly different, the calibration constant of the SDC position sensor was estimated to be 2000 V/m [14]. The present work is not so concerned with the actual magnitudes of the low-frequency oscillations seen in the figures, but rather with the fact they are observable.

All data were collected with a Dataq 700 (USB) 16-bit A/D converter, connected to a notebook (Windows 98) computer. The noise properties of a notebook were found generally superior to that of benchtop computers.

The more than score of figures which follow illustrate the low-frequency capabilities of the modified Sprengnether. Any significant originality that may be ascribed to these figures derives from the existence of the ‘synergetic triad’ that was part of their generation. This triad comprises: (i) a good sensor/instrument, (ii) an adequate interface, and (iii) a powerful but user-friendly data analysis package. The absence of any one of these three elements makes the generation of such figures impossible.

Although sensors have existed for years that could probably have been used in similar manner to the present work, what was not possible a generation ago were a matched set of items (ii) and (iii). Good interfaces existed more than a decade ago, in the form of A/D boards that slid into the case of a desktop computer. The software, however, with which one studied the stored records produced by these boards – was primitive. Generally, one had to write his/her own (dos) specialized code to learn much of anything from those records. In this author’s fairly extensive experience, only with the software/hardware combination sold by Dataq Inc., has the triad reached a mature state that far exceeds earlier *modus operandi*.

All figures were produced with the Dataq software that comes free with all of their interface instruments, starting with their \$25 10-bit A/D converter. Their code is very user-friendly and ideally suited to ‘exploratory’ analyses concerned with spectra. Especially useful is the means with which to easily view a complete 24-h record by means of time-compression of the data. ‘Compression’, as presently used, is equivalent to ‘input averaging’ in Dataq’s terminology.

Compression is necessary to identify low frequency oscillations that may be present in a record. Typically, to identify such a mode, the amount of compression used would be an integer (odd) in the neighborhood from 11 to 33. Likely places for the occurrence of such a mode are selected by first looking at the ‘maximum’ compressed waveform. Going back and forth between a compression of 1 and the maximum allowed by the software is trivial, using a ‘click of the mouse button’.

Once the code has been mastered, it is straightforward to do rapid analyses in either time or frequency. The use of the FFT and its inverse permits easy manipulation of the data to include (i) low-pass, (ii) high-pass, and (iii) band-pass filtering. Mastery is not especially difficult, being windows based. For all time displays of the present document that involved filtering, it was the band-pass filter that was used.

All data were collected at a sample rate of 8 per s, and all spectra were generated using the Hanning window (apodizing function), working with 2048 pt Fast Fourier transforms. Where bandpass filtering was employed, it was accomplished in two steps: (i) selecting the lower frequency cutoff of a ‘high-pass’ operation, followed by the inverse FFT, and (ii) selecting the higher frequency cutoff of a ‘low-pass’ operation, followed by the inverse FFT.

The figures were generated by (i) screen-printing a given Dataq display to the clipboard of the computer, and (ii) opening by ‘paste’ to the Windows routine ‘Paint’. For purpose of integration into the latex document from which this pdf was constructed, they were saved from paint as a ‘jpg’. Conversions were by means of code supplied with the freeware, ‘miktex’.

## References

- [1] Erhard Wielandt, “Seismic Sensors and their Calibration”, (section “Electronic displacement sensing”) a chapter of the *new Manual of Observatory Practice*, editors Bormann & Bergmann. Online at <http://www.geophys.uni-stuttgart.de/seismometry>
- [2] R. D. Peters, “Friction at the mesoscale”, *Contemporary Physics*, vol. 45, no. 6, 475-490 (2004).
- [3] R. D. Peters & T. Pritchett, “The not-so-simple harmonic oscillator”, *Amer. J. Phys.* vol. 65, no. 11, 1067-1073 (1997).
- [4] R. D. Peters, “Nonlinear damping of the ‘linear’ pendulum” online at <http://arxiv.org/pdf/physics/0306081>
- [5] R. Peters & L. Sumner, “Intuitive derivation of Reynolds number”, online at <http://arxiv.org/html/physics/0306193>
- [6] A. Kimball & D. Lovell, “Internal friction in solids”, *Phys. Rev.* 30, 948-959 (1927).
- [7] private communication from E. Wielandt.
- [8] “Vibration and Shock Handbook”, ed. C. de Silva, CRC Press, ch. 20, (2005).
- [9] T. Erber, “Hooke’s law & fatigue limits in micromechanics”, *Eur. J. Phys.* vol. 22, no. 5, 491-499 (2001).
- [10] R. D. Peters, “Metastable states of a low frequency mesodynamic pendulum”, *Appl. Phys. Lett.* 57, 1825 (1990).
- [11] R. D. Peters, “The pendulum in the 21st century—relic or trendsetter?” *Sci. & Educ.* 13, Nos. 4-5 (2004).
- [12] P. Bak, C. Tang, & K. Wiesenfeld, “Self-organized criticality, An explanation of 1/f noise”, *Phys. Rev. Lett.* 59, 381-384 (1987). Also, same authors, *Phys. Rev. A*, 38, 364-374 (1988), and *J. Geophys. Res.* 94, 15,635-15,637 (1989).
- [13] “Symmetric differential capacitance transducer employing cross coupled conductive plates to form equipotential pairs”, U.S. Patent No. 5,461,329 (1995).
- [14] see, for example, the online page <http://physics.mercer.edu/earthwaves/instr.html>

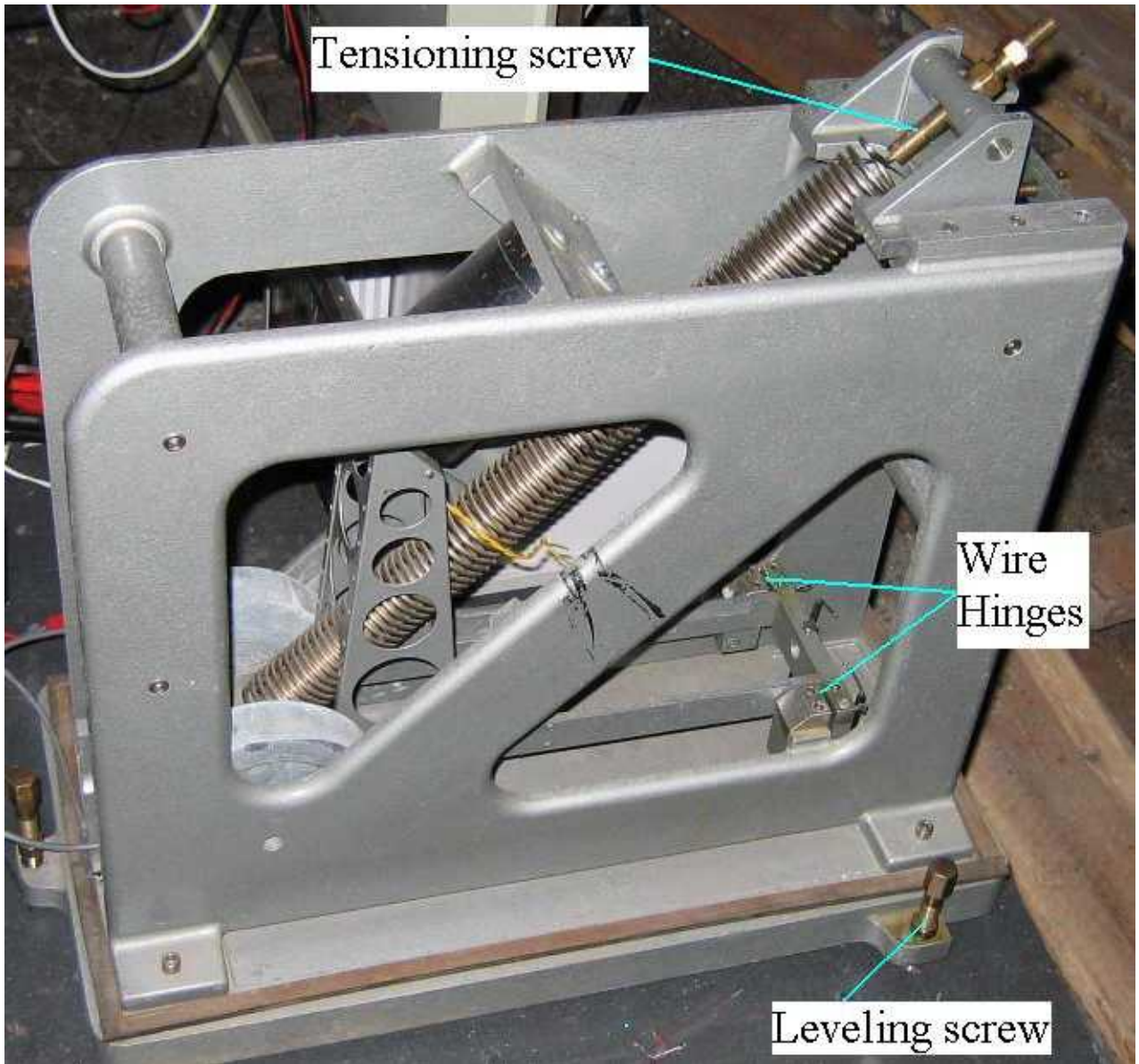


Figure 1: Long-period vertical seismometer, manufactured by Sprengnether, that was once part of the WWSSN.

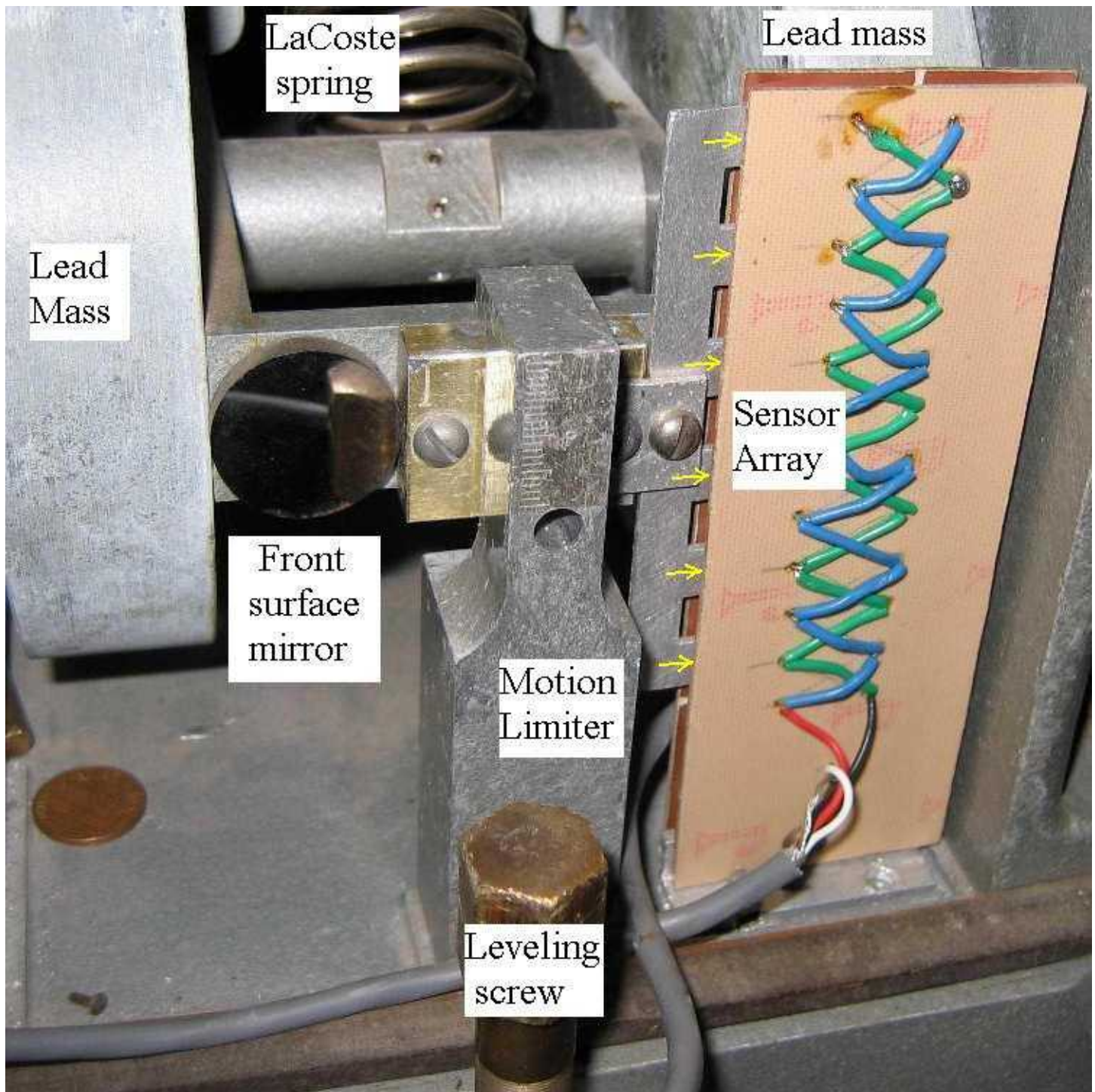


Figure 2: Six-element area-varying capacitive array used as the sensor in the modified instrument.

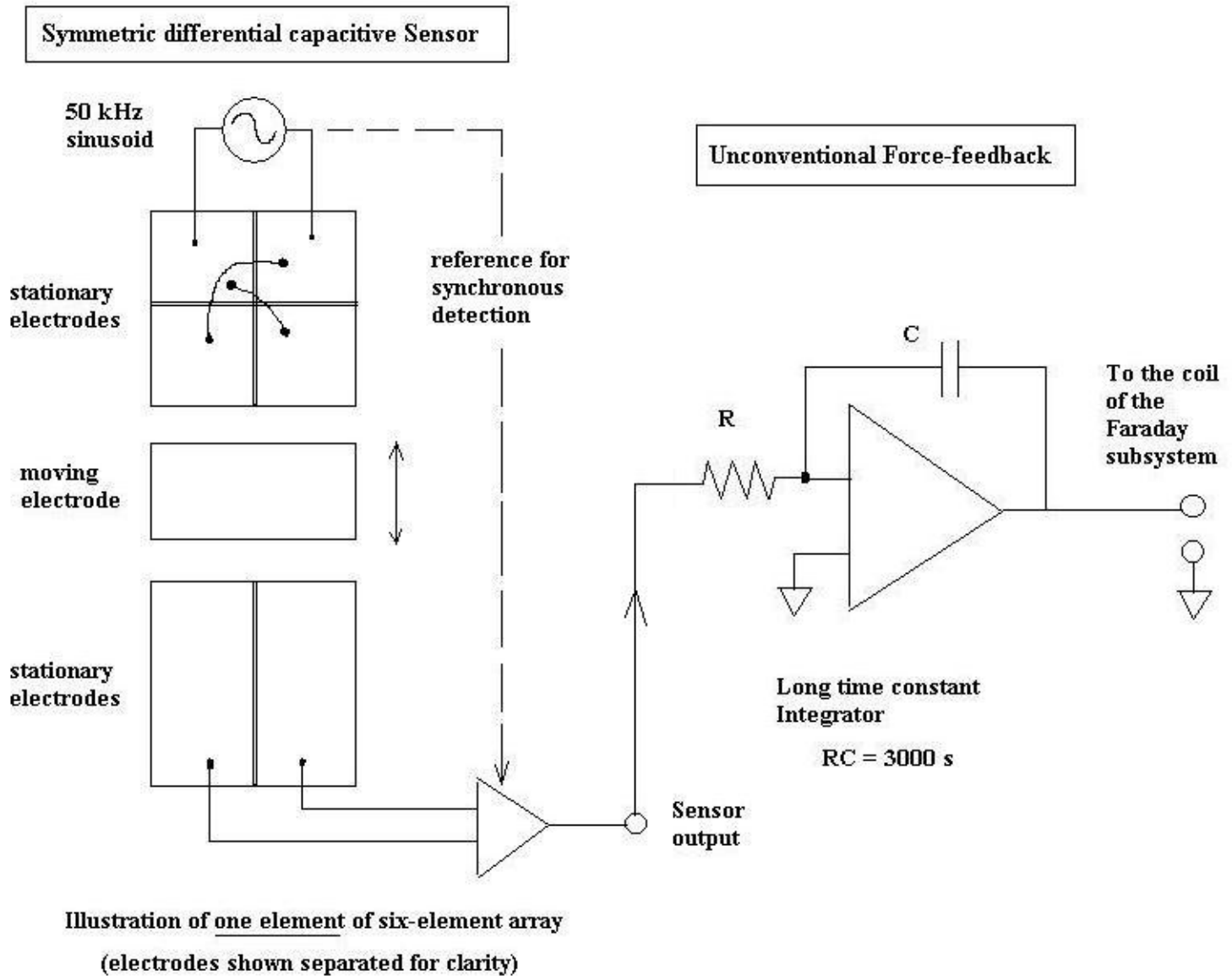


Figure 3: Electronics diagram for the modified Sprengnether.

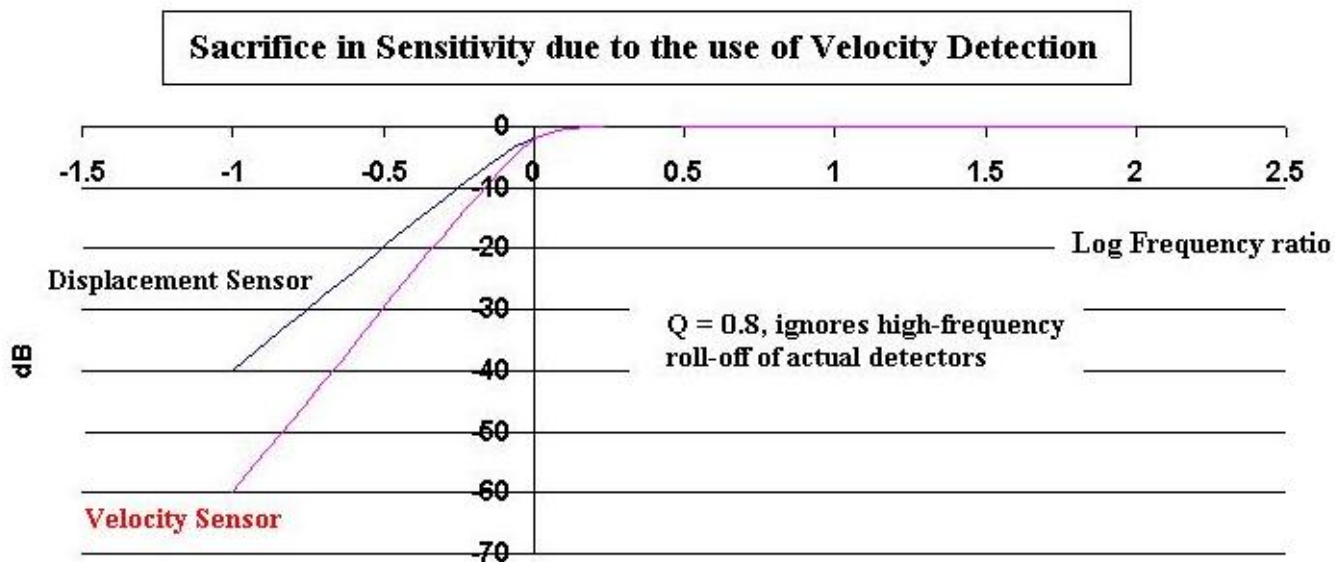


Figure 4: Bode plot showing why velocity detection is not used.

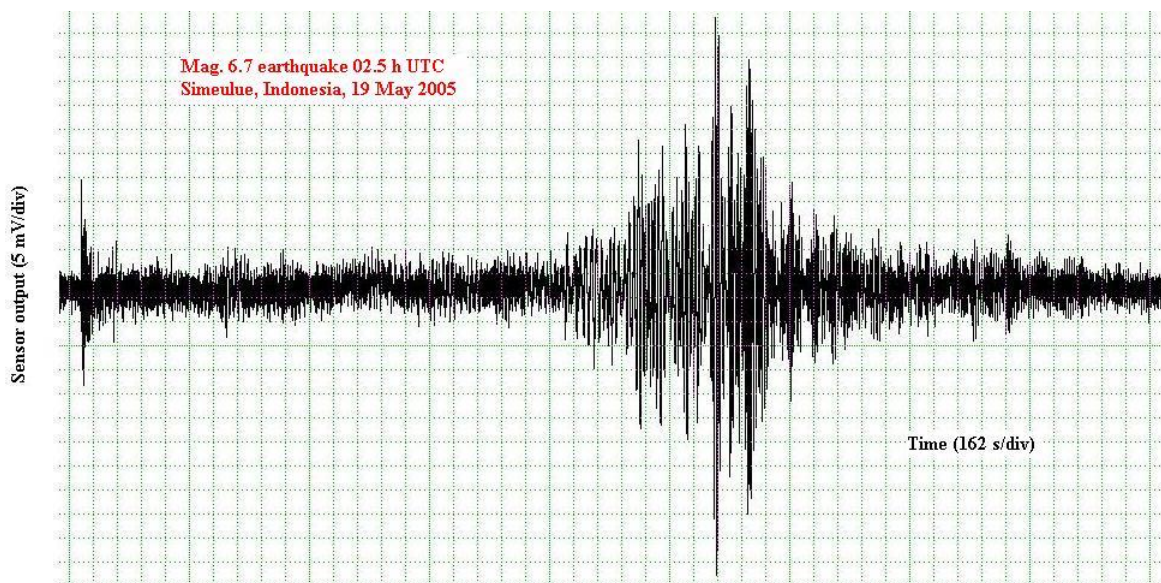


Figure 5: Compressed-time Record of Indonesian earthquake, 19 May 2005.

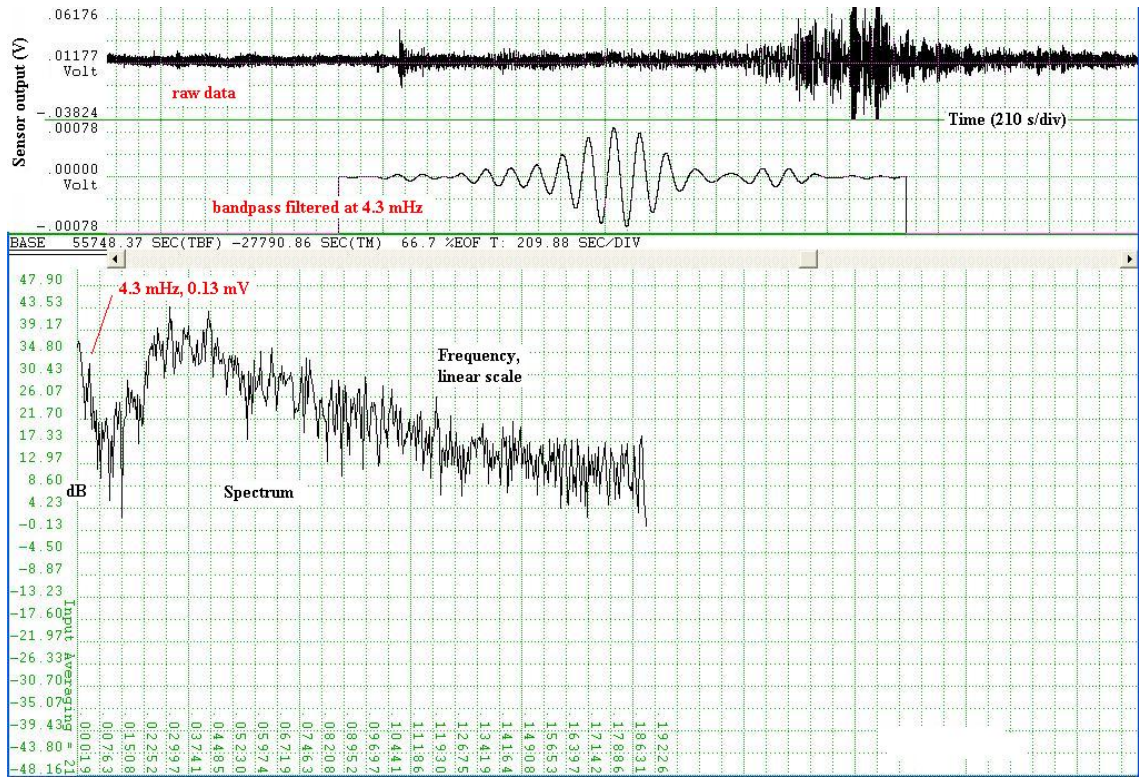


Figure 6: Low frequency oscillation in interval between body-waves and surface waves.

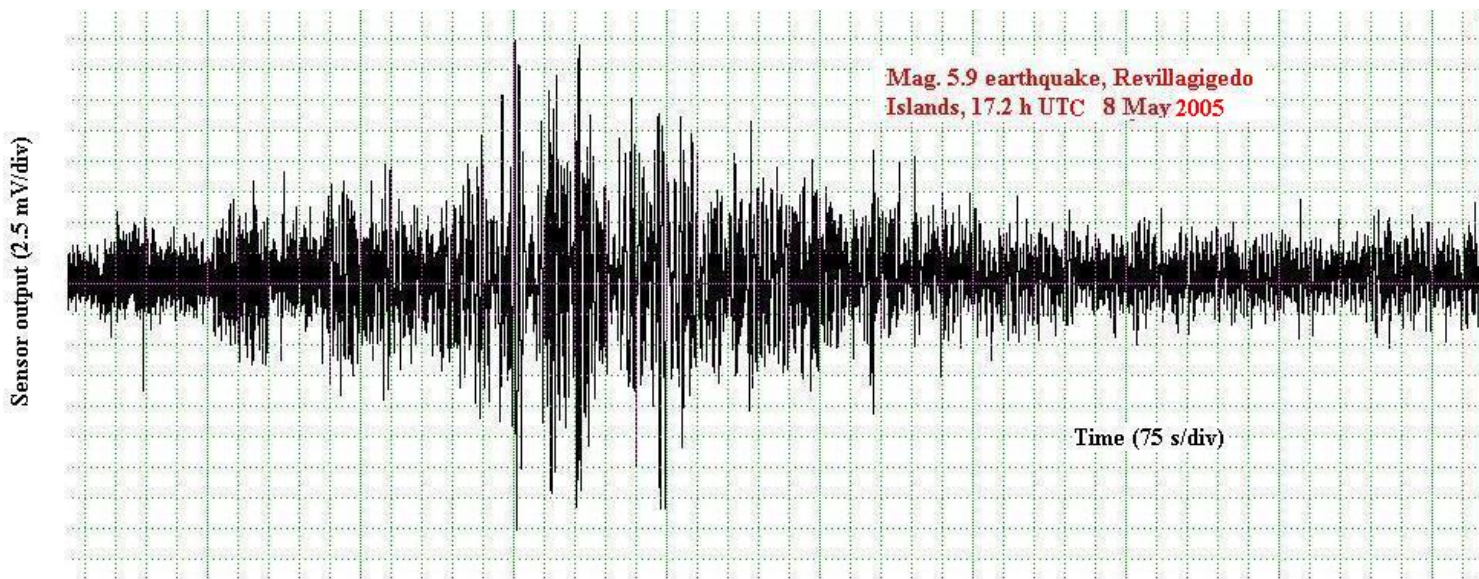


Figure 7: Compressed Earthquake record, Revillagigedo Islands, 8 May 2005.

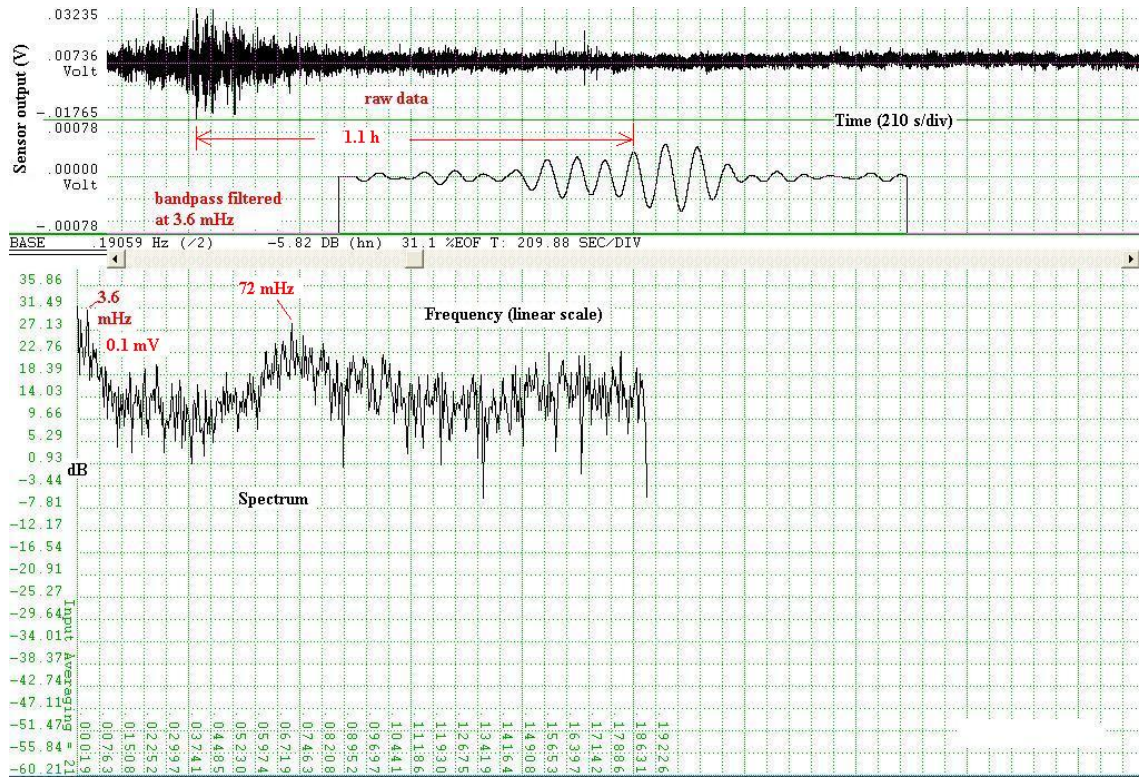


Figure 8: Oscillation at 3.6 mHz following the Revillagigedo earthquake.

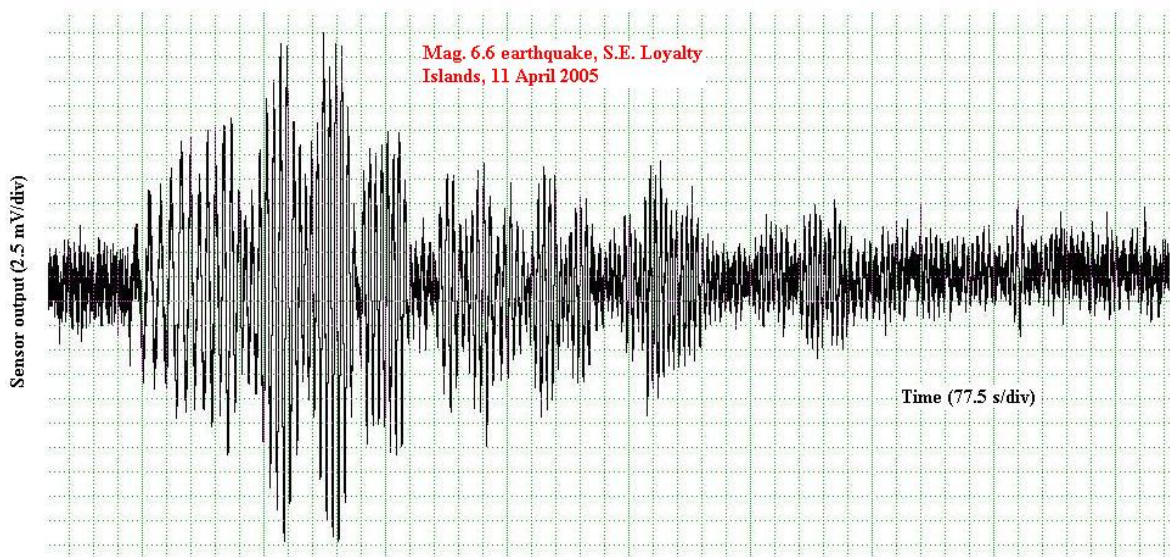


Figure 9: Compressed Earthquake record, Southeast Loyalty Islands, 11 April 2005.

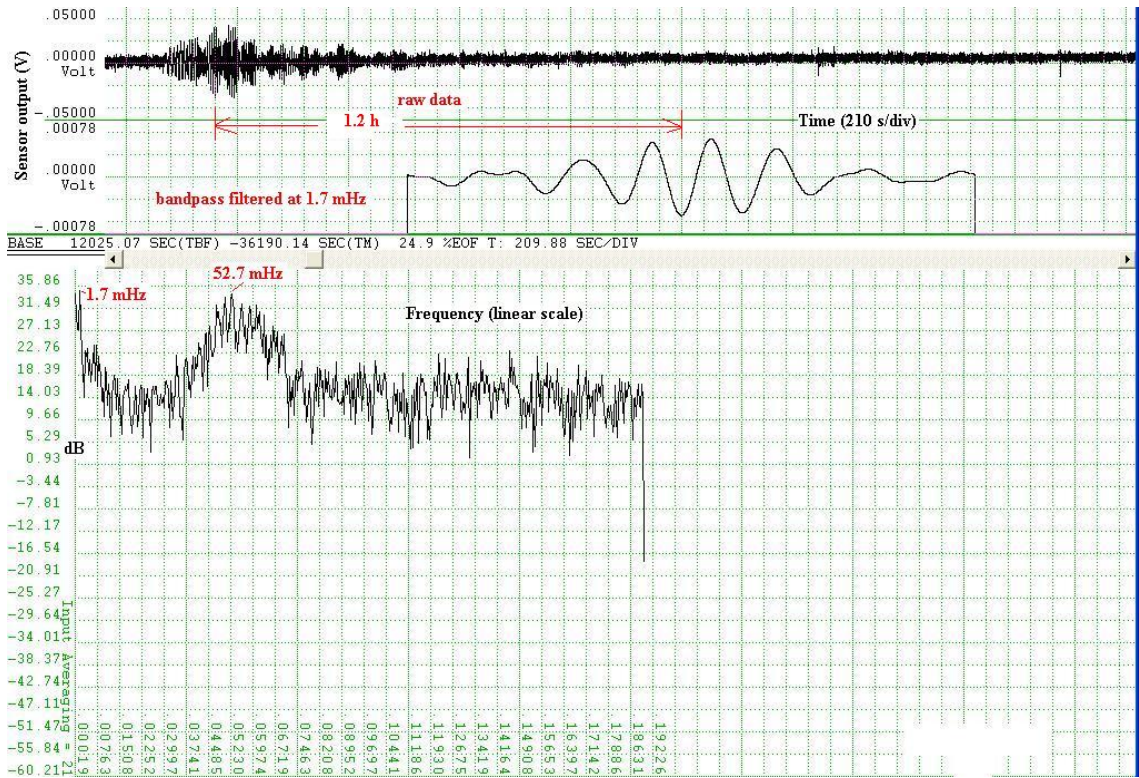


Figure 10: Oscillation at 1.7 mHz following the Loyalty Is. earthquake.

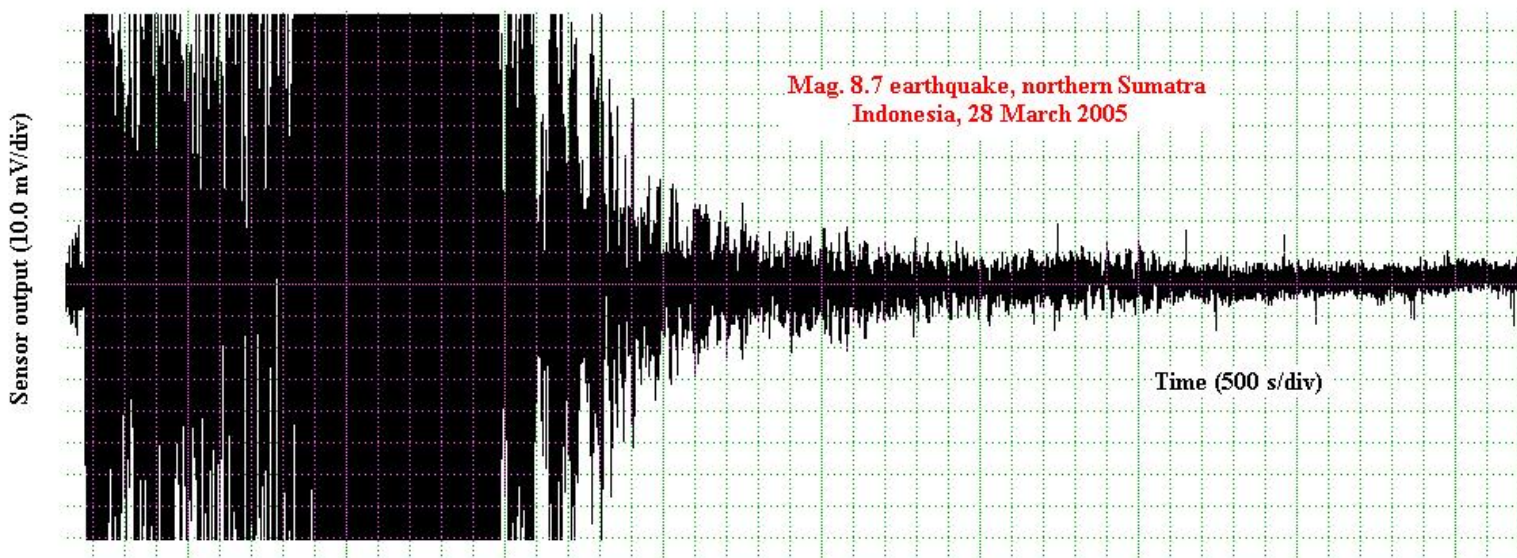


Figure 11: Clipped waveform of the very large Nias earthquake of 28 March 2005.



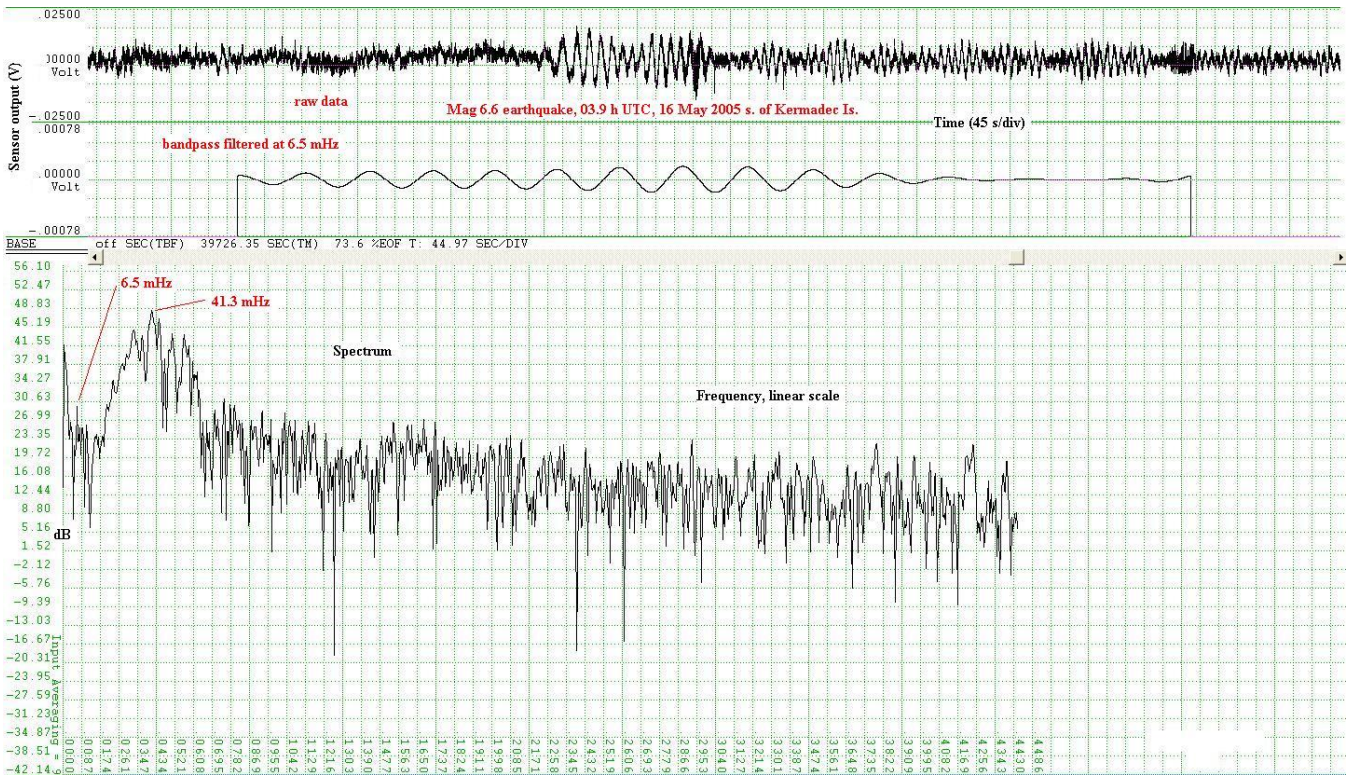


Figure 14: Earthquake (Kermadec Islands), following unusual pre-cursor activities (11.0 h after 'event').

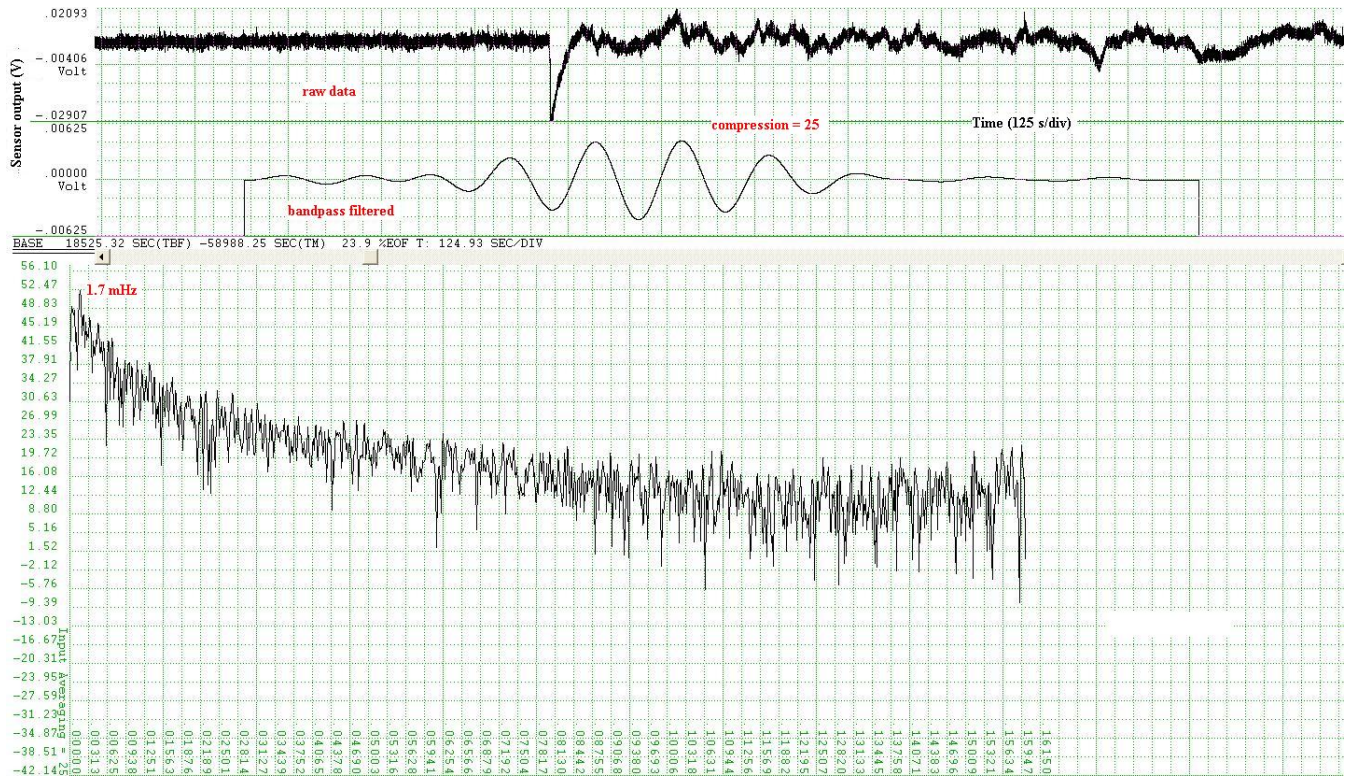


Figure 15: One example of pre-earthquake oscillation (0.33 h after 'event').

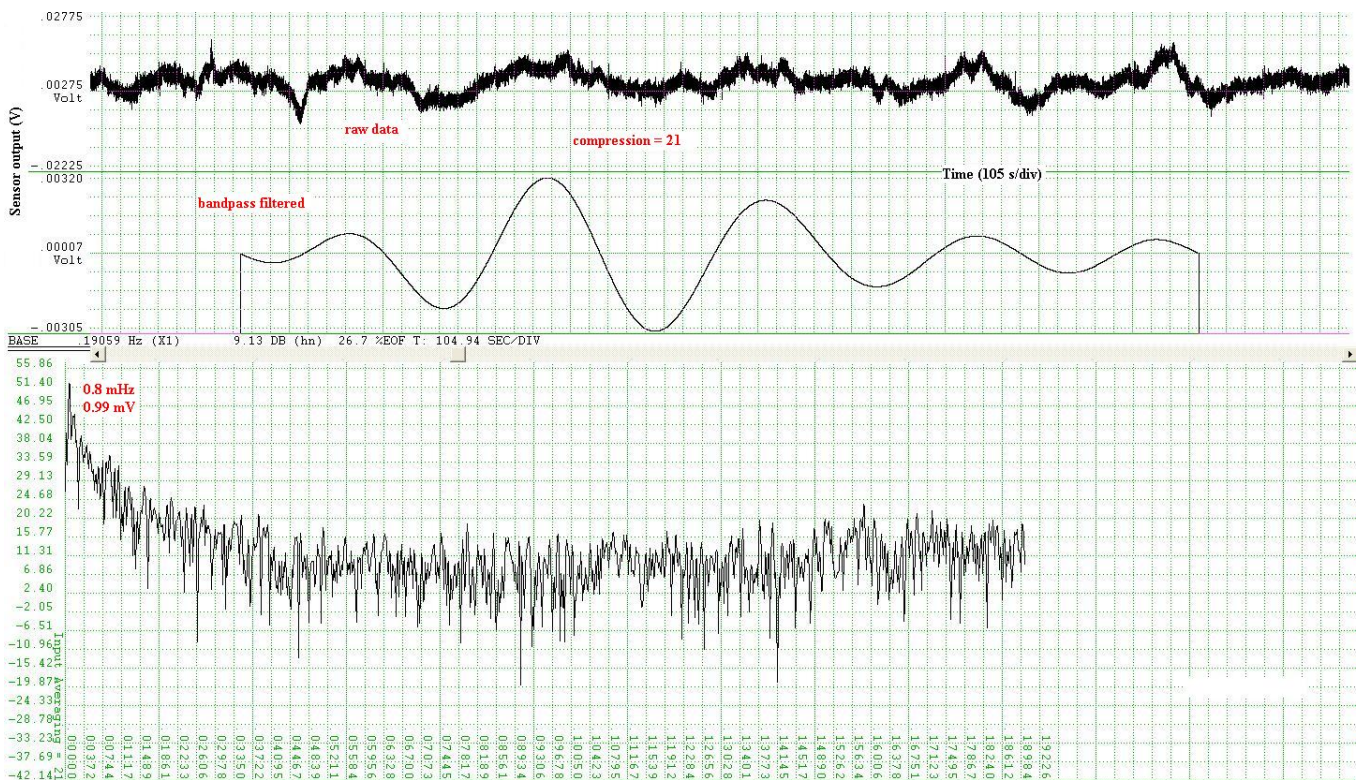


Figure 16: Second example of pre-earthquake oscillation (1.7 h after 'event').

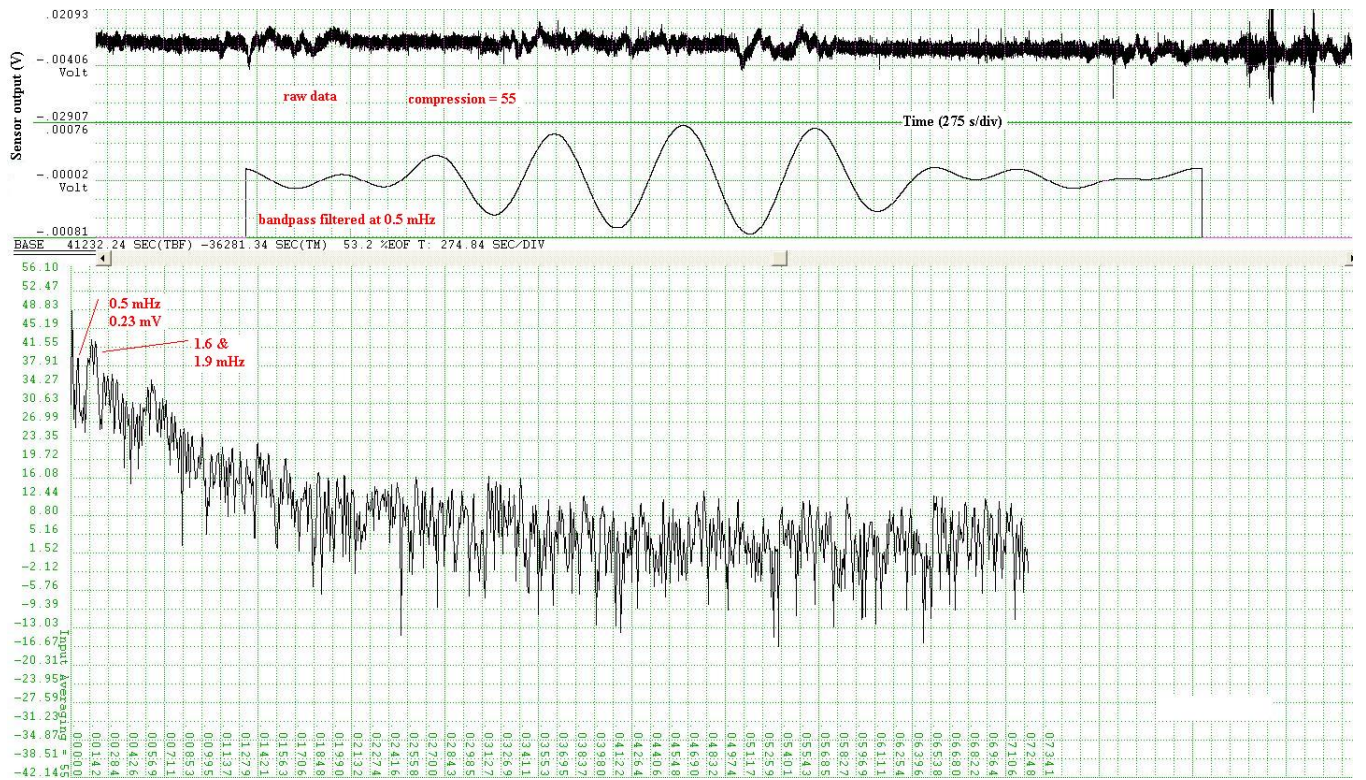


Figure 17: Third example of pre-earthquake oscillation (6.6 h after 'event').

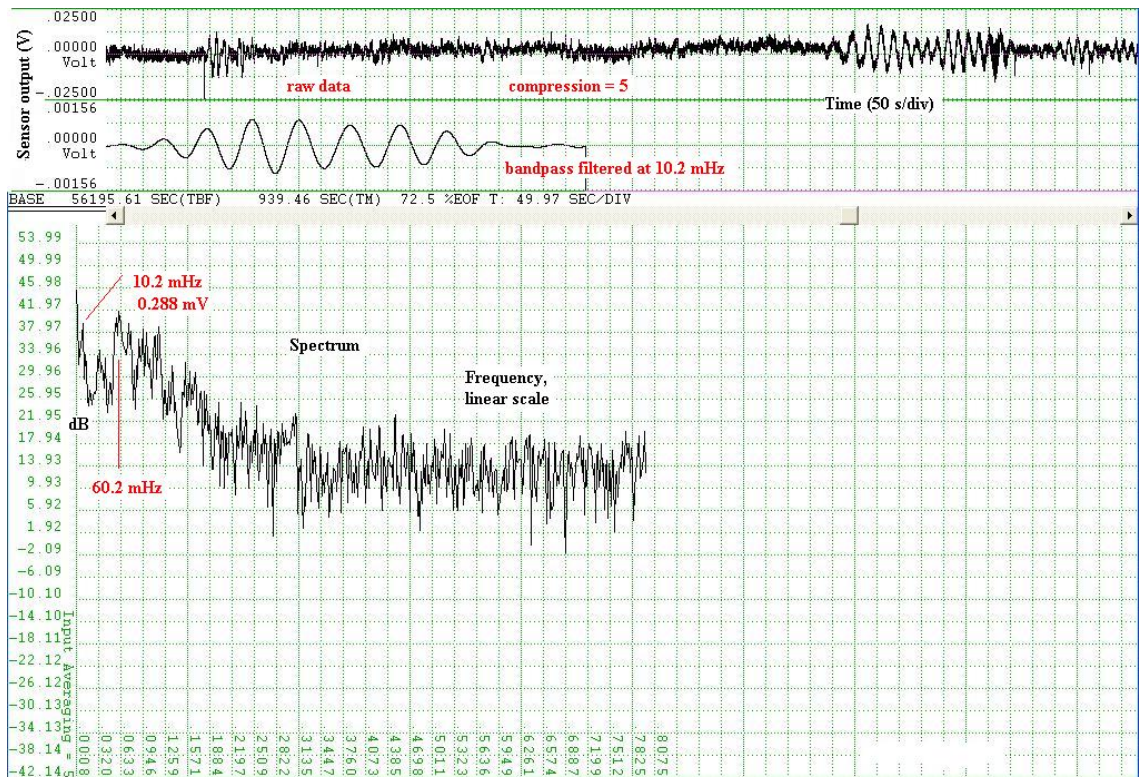


Figure 18: Oscillation before arrival of the surface waves (10.6 h after 'event').

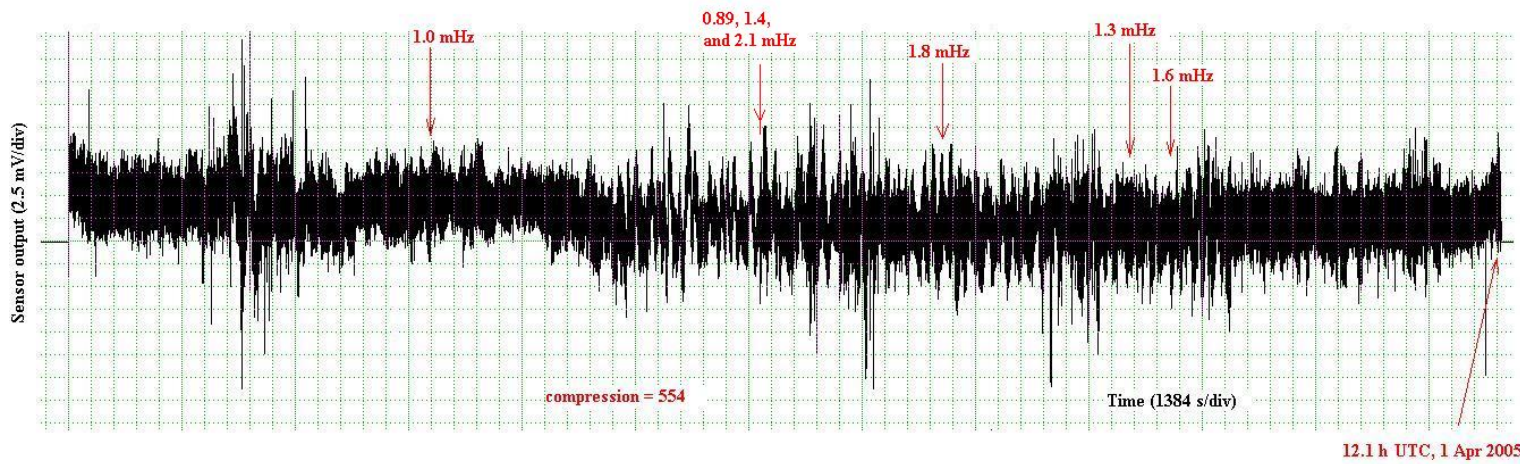


Figure 19: 24-h record during period of minimal earthquake activity, yet showing many low-frequency oscillations.

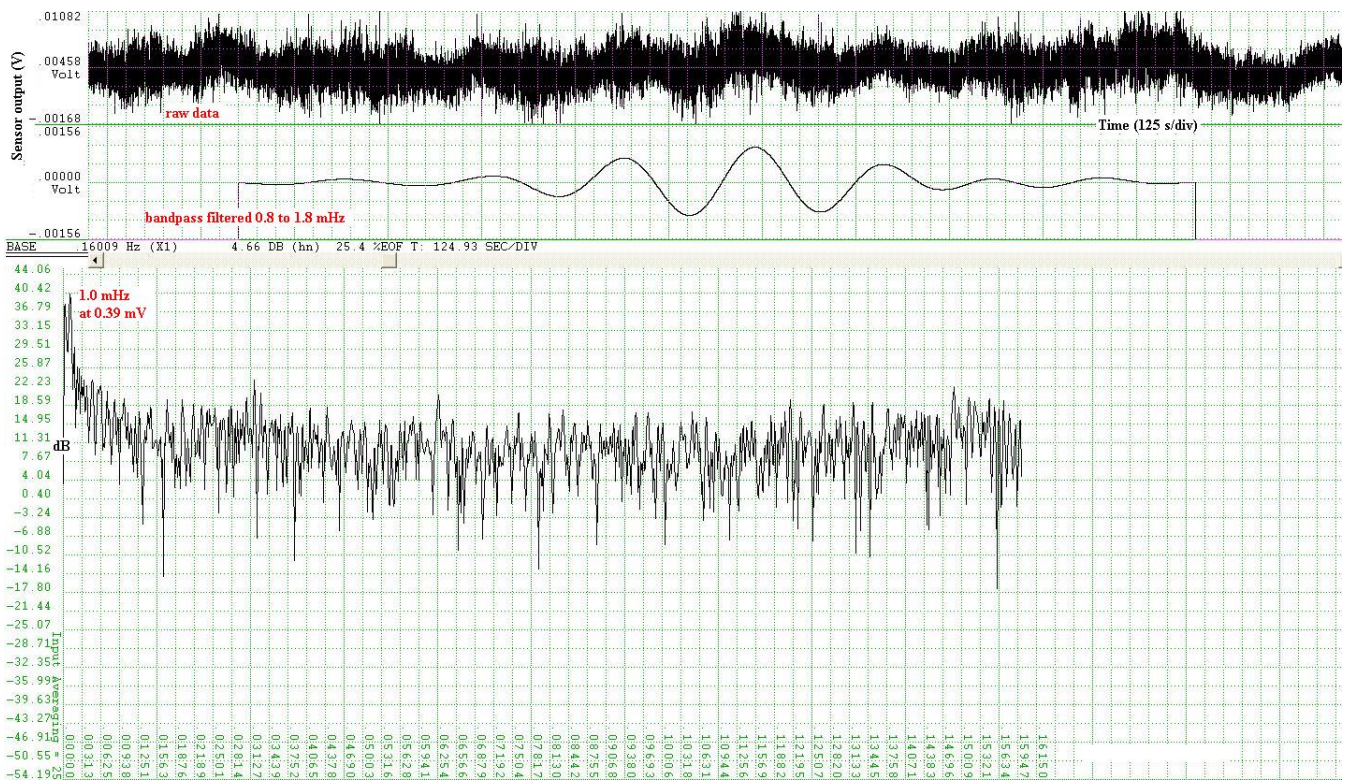


Figure 20: The first-noted low frequency oscillation of fig.(19).

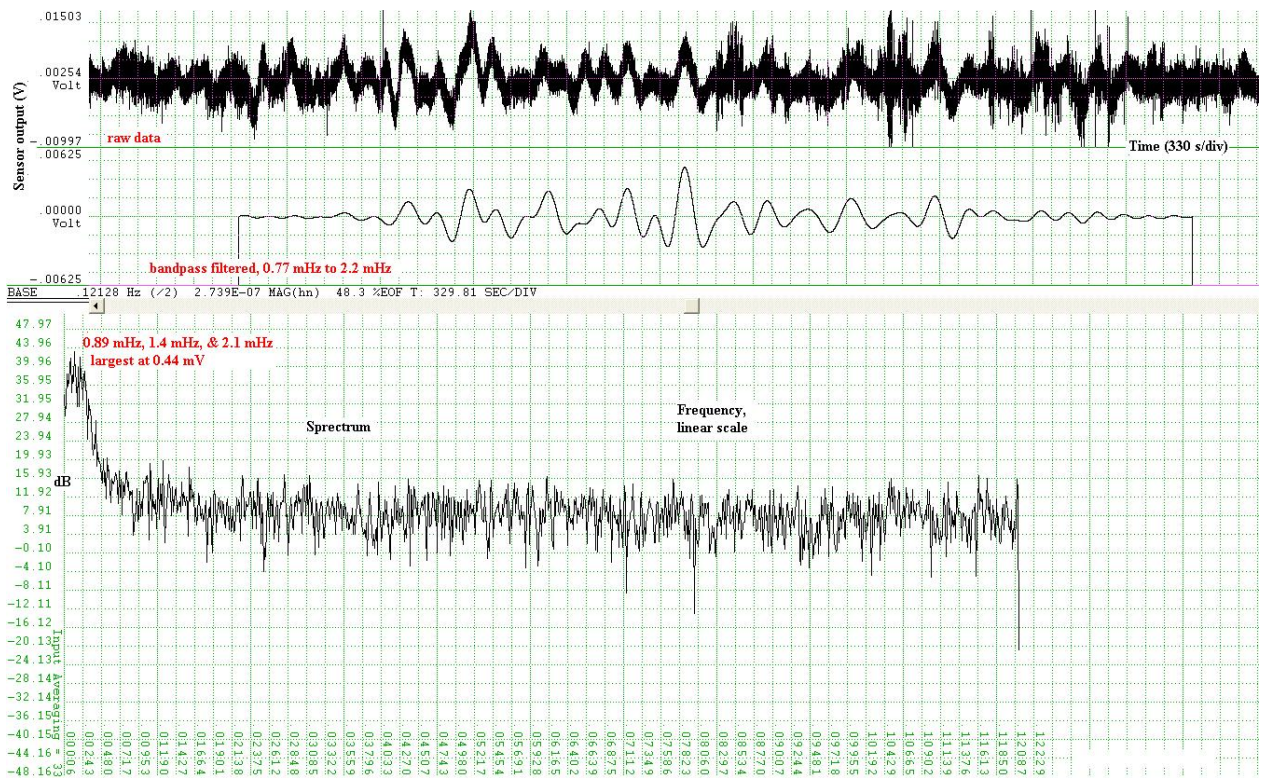


Figure 21: The second-noted, low frequency group of oscillations, of fig.(19).

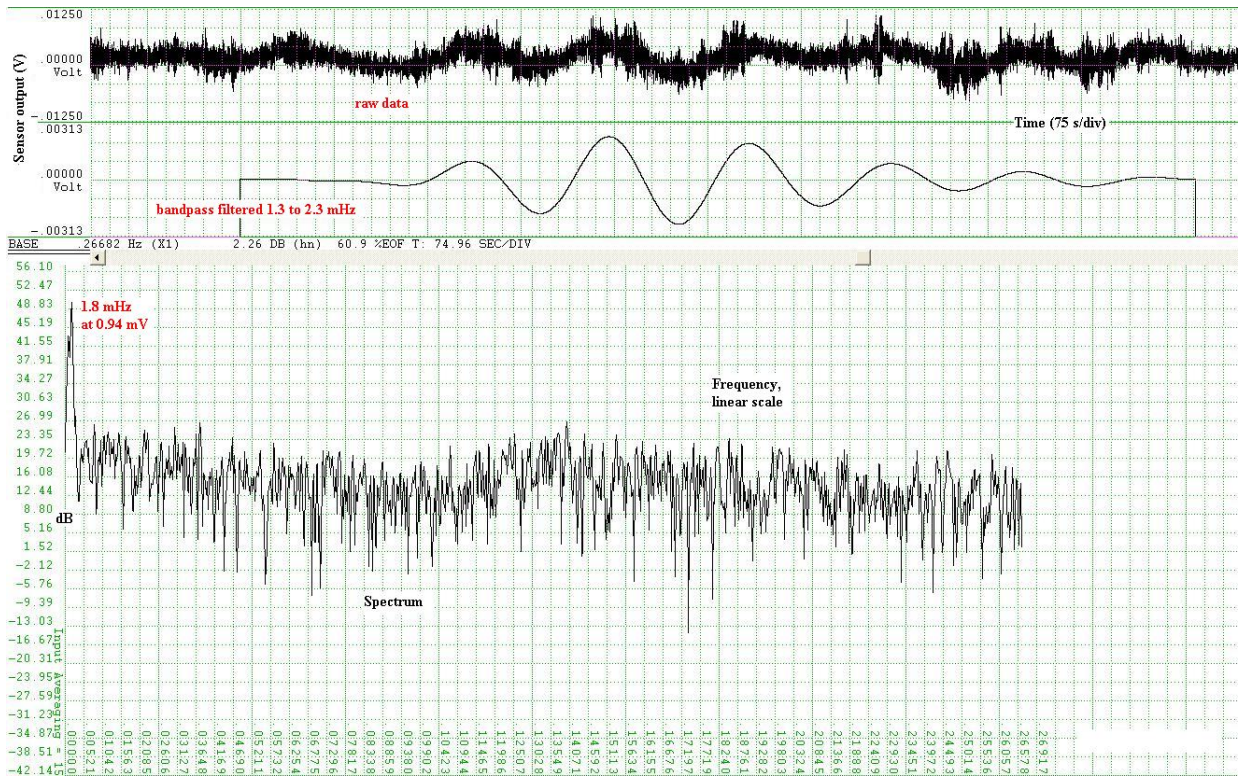


Figure 22: The third-noted low frequency oscillation of fig.(19).

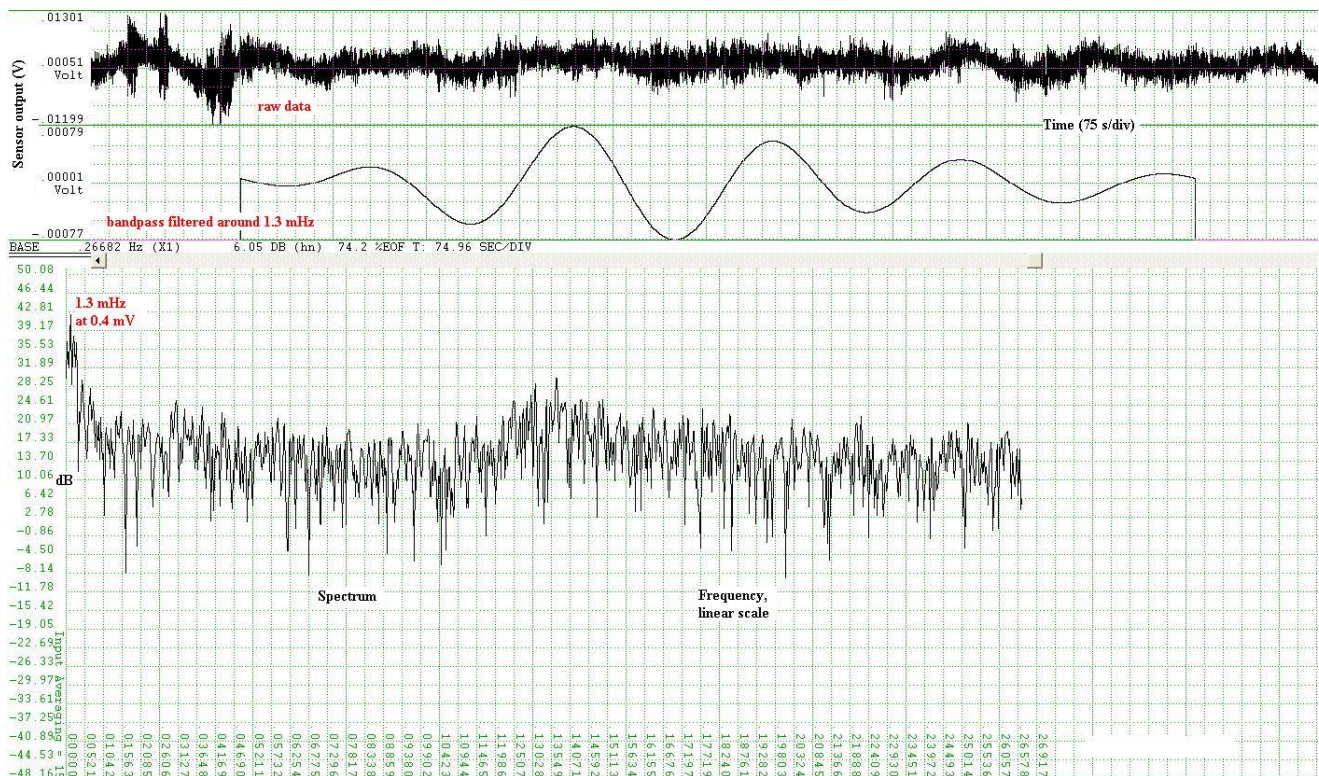


Figure 23: The fourth-noted low frequency oscillation of fig.(19).

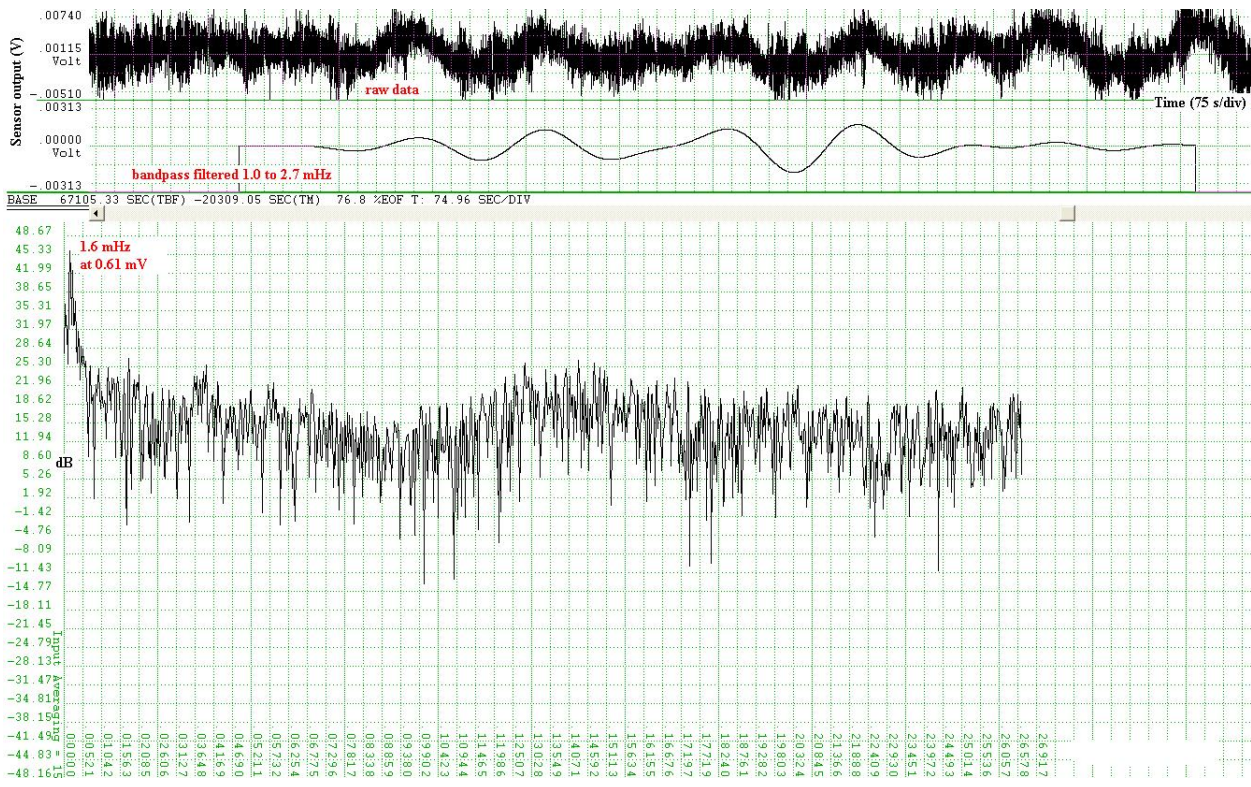


Figure 24: The fifth-noted low frequency oscillation of fig.(19).